Energy, Mines and Resources Canada | Énergie, Mines et Ressources Canada

CANMET

Canada Centre for Mineral and Energy Technology | Centre canadien de la technologie des minéraux et de l'énergie

EFFECT OF THICKNESS ON FATIGUE LIFE OF WELDED PLATE T-JOINTS

O. VOSIKOVSKY and A. RIVARD
ENGINEERING PHYSICS SECTION

NOVEMBER 1985

PHYSICAL METALLURGY RESEARCH LABORATORIES

This document is an unedited interim report prepared primarily for discussion and internal reporting purposes. It does not represent a final expression of the opinion of the Canada Centre for Mineral and Energy Technology (CANMET)

Ce document est un rapport provisoire non-révisé et rédigé principalement à des fins de discussion et de documentation interne. Il ne représente nullement l'opinion définitive du Centre canadien de la technologie des minéraux et de l'énergie (CANMET)

REPORT: PMRL 85-65(TR)

PHYSICAL METALLURGY RESEARCH LABORATORIES
REPORT: PMRL 85-65(TR)

EFFECT OF THICKNESS ON FATIGUE LIFE OF WELDED PLATE T-JOINTS

by

O. Vosikovsky and A. Rivard

ABSTRACT

The fatigue lives and the development of fatigue cracks in welded plate steel T-joints 16, 26, 52, 78 and 103 mm thick are reported.

The joints were tested at constant amplitude loading at the following three stress ranges: 100, 150 and 200 MPa.

The fatigue crack growth was monitored by multiprobe AC potential drop and beach marking techniques.

LABORATOIRES DE RECHERCHE EN MÉTALLURGIE PHYSIQUE
RAPPORT: LRMP 85-65 (TR)

EFFET DE L'ÉPAISSEUR DE L'ACIER SUR LA DURÉE DE VIE DES JOINTS EN T

par

O. Vosikovsky et A. Rivard

RÉSUMÉ

Le rapport porte sur la durée de vie et la croissance de fissures par fatigue de joints en T en acier d'une épaisseur de 16, 26, 52, 78, et 103 mm.

Les joints ont été soumis à des essais à contrainte imposée de 100, 150, et 200 MPa.

La croissance des fissures par fatigue a été suivie par la mesure en plusieurs points de la différence de potentiel en courant alternatif et par la technique des lignes d'arrêt.

INTRODUCTION

The deleterious effect of increasing section thickness on fatigue life of welded joints has been recognized for several years, and recently was included in modified fatigue design rules for offshore structures [1].

The effect of thickness up to 100 mm has been intensively studied in tests of welded cruciform or T-plate joints with non-load carrying welds loaded either in tension [2] or in three or four-point bending [3-6].

The present experimental work is carried out on plate T-joints, 16-103 mm thick, with load carrying welds. Load is applied through attachment plates to simulate loading of tubular joints in offshore structures. Because to date, in the work of others, the thickness effect has only been studied in air, information on the applicability of size effect derived from tests in air to corrosion fatigue in sea water, with and without cathodic protection, is lacking.

Thus, the CANMET research program concentrates on evaluation of the size effect in sea water at free corrosion, optimum cathodic protection, and cathodic over-protection. Part of the experimental program (reported here) is carried out at PMRL/CANMET; the other part (reported separately) is contracted to AMCA Int. and the University of Waterloo.

In this report the basic PMRL data from completed tests on the size effect in air are reported. These data will later be combined with those from the University of Waterloo and analyzed in terms of S-N curves in a comprehensive report. The fracture mechanics analysis of the PMRL tests, and a comparison with a life prediction model developed under CANMET contract with Carleton University, has been reported already [7]. Corrosion fatigue tests are in progress.

MATERIAL AND WELDING OF T-JOINTS

The geometry and dimensions of the test T-joints, 16, 26, 52, 78 and 103 mm thick, are given in Fig. 1. The chemical composition and mechanical properties of the steel plates used to fabricate the specimens are listed in Table 1. The plates 26, 52 and 78 mm thick, manufactured to Lloyd's LT60

specification, were rolled from the same heat and normalized. The 16 and 103 mm plates were manufactured to CSA 640.21 Grade 350 WT specification. The 16 mm plate was control rolled. The 103 mm plate, cast as an ingot, was supposed to have been normalized but was tested in the as-rolled condition by error. Thus, it had a fairly coarse ferrite grain (40 μm mean diameter close to the surface, 63 μm close to the centre thickness).

The test T-joints were manually welded with full penetration by a balanced welding technique. Nominally 45° welds were deposited in the vertical up (3G) position with no restraints. The weld preparation and a typical pass sequence for 26 mm thick plate are shown in Fig. 2. The welding parameters are listed in Table 2. The weld-toe profile was controlled by the "dime" test. The "dime" test requires that when a disc of radius equal to one half of the plate thickness is placed against the weld toe and the longitudinal plate, a 1 mm diameter wire cannot pass between the disc and plate. This welding procedure was adopted from the United Kingdom Offshore Steel Research Project (UKOSRP) Phase II. The specimens were tested in the as-welded condition.

Before testing, the weld-toe geometry characterized by radius r, and angle θ, were measured on sectioned plaster or RTV rubber casts of weld profiles. Ten measurements have been made for each weld, on sections spaced at 20 mm, on 5X magnified photographs of cast cross-sections.

EXPERIMENTAL PROCEDURES

Test conditions

The T-joints were tested in 3-point bending in specially designed frames, equipped with MTS controls and actuators of 100, 250 and 500 kN capacity. Loads were applied through pin connections to the attachment plate. To achieve proper alignment of specimens which were often warped by welding, the position and tilt of the reaction beams were adjusted by two set screws as shown in Fig. 3.

The alignment of each specimen was checked by two strain gauges attached to the centre of the base plate 20 to 40 mm from the weld toes. Larger distances were used for thicker joints to ensure that the gauges were

outside the local stress concentrations of the weld. One specimen of each thickness was instrumented with a strip gauge to measure the effect of thickness on stress distribution near the weld toe. Strain measurements were done at incrementally increased loads after application of about 200 cycles at the same loads used in subsequent fatigue testing.

Fatigue testing was conducted in laboratory air at constant amplitude loading with a load ratio R = 0.05, and at the highest achievable cyclic frequency of 4 to 20 Hz. The highest frequencies were used for thin joints tested at low stresses. During the tests, crack growth and actuator displacement range were monitored.

Fatigue crack growth monitoring

A combination of AC potential drop (ACPD) measurements and beach marking were used to determine the maximum depth and the shape of fatigue cracks. ACPDs were measured with a Unit Inspection Crack Micro-Gauge [8]. Eighteen probe pairs were spot welded at 10 mm spacing (see Fig. 1) along one weld toe and periodically monitored throughout the test. Only two reference probes located one quarter width distance from joint edges, near active probes No. 5 and 15, were used. The potential signal was fed into the Micro-Gauge through a 20 channel low voltage switching unit (Fig. 3). The amplified DC signal from the Micro-Gauge was linked to a computer. To ensure that the fatigue cracks grew from the instrumented weld toe, the weld toe on the opposite side of the attachment plate was ground to remove defects and reduce the stress concentration.

For uniform current field distribution and a straight-fronted crack, the crack depth can be calculated from the following equation [8]:

$$a = \frac{\Delta}{2}\left(\frac{V}{Vo} - 1\right) \qquad \text{Eq 1}$$

where Δ = 10 mm is the probe length, V is the potential across the crack, and Vo is the reference potential next to the crack. For the spot welded probes located across the weld toe the initial ratio of $\left(\frac{V}{Vo}\right)_{a=0}$ was not equal to one and the equation (1) was modified to:

$$a = A\left[\left(\frac{V}{Vo}\right)_a - \left(\frac{V}{Vo}\right)_{a=o}\right] \qquad \text{Eq 2}$$

where A is a calibration coefficient.

To determine the calibration coefficient A for semi-elliptic multiple cracks, growing from the weld toes, four to six beach marks were produced on each specimen. The first beach mark was made by ink staining when the maximum crack depth reached 2-4 mm. The subsequent beach marks were made by reducing the load range 50% and doubling the frequency for an appropriate number of cycles to produce a small crack extension. These beach marks were produced after 3-8 mm crack depth increments. Use of calibration curves, consisting of linear segments connecting the beach mark calibration points, gave an estimated accuracy of ±0.5 mm in determining crack depth measurements by the ACPD technique. Examples of the calibration curves for the probes nearest to the deepest point of the crack in four specimens (26 and 78 mm thick and tested at 100 and 200 MPa stress ranges) are given in Fig. 4. For small, close to semi-circular cracks, particularly at low stress ranges where only a few cracks start, the initial rate of increase of PD with crack depth was apt to be lower than the assumed linear interpolation. As a result, the reported maximum crack depths below 2 mm may be underestimated by as much as 0.5 mm.

EXPERIMENTAL RESULTS

Weld toe geometry

The results of measurements of weld geometry on single specimens in terms of leg length ℓ, minimum, maximum, and mean weld toe angle $\bar{\theta}$ and weld toe radius $\bar{r}$ are presented in Table 3. As indicated by the spread between maxima and minima and the values of standard deviations S_θ and S_r, both the angle and radius vary widely along the length of welds. However, the mean values for single specimens are reasonably consistent. For all joints tested, the mean value of $\bar{\theta} = 41.3°$, and mean radius $\bar{r} = 1.39$ mm.

Stress distribution near weld toe

The weld toe stress distributions measured by strip gauge on one specimen of each thickness and subsequently fatigue tested at the nominal weld toe stress range $\Delta\sigma$ = 150 MPa are presented in Fig. 5. The stresses were converted from measured strains by simple multiplication by Young's modulus E = 210 GPa, and for consistency with subsequent fatigue test, are presented in terms of stress range $\Delta\sigma$ (R = 0.05). The $\Delta\sigma$ at the weld toe has been calculated from simple beam theory and verified by linear extrapolation of measurements from strain gauges placed at a minimum distance of 20 mm i.e. outside the local stress concentration of the weld. The extrapolated values of $\Delta\sigma$ are presented in Table 4.

The local stress distributions measured near the weld toe at a constant nominal stress range $\Delta\sigma$ = 150 MPa are shown in Fig. 5. They reveal that the spread of highly concentrated stresses increases with increasing plate thickness. Because the span was roughly proportional to plate thickness (see Fig. 1), the single curves do not join further away from weld toe.

When the distance x from weld toe is normalized by dividing it by specimen thickness t, the measured stresses for all thicknesses fall in a narrow scatter band, as shown in Fig. 6. Local stress concentration disappears beyond the distance of 0.1 t from the weld toe.

Fatigue life

Endurance was defined as the number of cycles to reach a maximum crack depth of half the plate thickness. Beyond that point, both the crack-growth rate and the displacement range increase rapidly, and the ability of the specimen to carry load is practically exhausted.

Fatigue crack initiation was arbitrarily defined as the number of cycles to reach a maximum crack depth a_i = 0.5 mm, as determined from a vs N curves fitted to experimental data.

Measured initiation and endurance lives are presented in Table 4, and Fig. 7. The stress ranges used in the S-N plot (Fig. 7) were the calculated but, as shown in Table 4, agree with measured (extrapolated) weld toe stress ranges to within ± 5% (although the extrapolated values tend to be systematically low).

Records of actuator displacement range $\Delta\ell$, showed that the first measurable increase in compliance range occurs relatively late in the fatigue life, after considerable crack growth. Steep increase in compliance occurs when the maximum crack depth approaches the specimen thickness. Examples of variation in $\Delta\ell$ with number of cycles and crack depth were presented in an interim report [9]. The number of cycles, and corresponding maximum crack depth for the first detectable steady increase in the displacement range of 0.01 mm, determined from curves fitted to measured data, are given in Table 5.

Crack growth measurements

A number of fatigue cracks initiated along the weld toe. Initially, their shape was close to semi-circular. As they grew deeper their shape changed to semi-elliptic with decreasing aspect ratio $\frac{a}{c}$ (where a is crack depth, c is surface half-length). The rate of decrease in aspect ratio was augmented by coalescence of single cracks. These observations were made from examination of beach marks. Examples of such beach marks on 26 and 78 mm thick specimens, tested at stress ranges of 100 and 200 MPa, are shown in Fig. 8a-d. Analysis of the number of cracks indicated by first (ink stain) beach marks, and their further development, indicated by subsequent marks in single specimens, shows that the number of initiated cracks increased with stress range and thickness. Hence, the rate of transition from initial semi-circular to straight-fronted cracks, dominated by crack coalescence, increased with stress range and thickness. Measurements of crack-shape development and its incorporation in fracture mechanics fatigue life predictions were reported in [7].

In addition to determinating crack-shape development, the beach marks were used for calibrating ACPD measurements. Comparisons of measured potential distributions at beach mark sites with the actual crack sizes are shown in Fig. 9a-f for specimen thicknesses of 26 and 78 mm and stress ranges of 100,

150 and 200 MPa. Note, that the left hand scales (for crack depth) are magnified by 10 and 5 times for 26 and 78 mm thick plates respectively, compared with the horizontal scales (for specimen width). For the AC potential scales (right hand axis), the value of A = 5 mm (half the probe distance) in Eq 2 was selected. With this value of A, Eq 1 or 2 should convert the potential into the left scale crack depth for a straight-fronted crack. As can be seen from Fig. 9f (T = 78 mm, $\Delta\sigma$ = 200 MPa), as a result of a high number of initiating cracks the main crack front was fairly straight (even for shallow cracks), the agreement between ACPD predicted and measured crack depth is reasonably good. However, for low stress ranges, where only few widely spaced cracks initiated, Fig. 9a (t = 26 mm, $\Delta\sigma$ = 100 MPa), the predicted crack depth for 3 mm deep cracks could be as low as one quarter of the actual depth. The agreement improves as cracks coalesce, and for larger semi-elliptic cracks close to 10 mm deep, the predicted crack depth is about one half the actual depth. Similar conclusions can be reached by comparing calibration curves in Fig. 4. This shortfall in the predicted length of semi-elliptic cracks is well known and corrections for crack curvature which improve the prediction accuracy for large cracks of known shape were proposed [8]. For small multiple cracks, as can be seen from the Fig. 9, the ACPD potential distribution cannot distinguish between one big crack or a group of small cracks. This shortcoming in the method makes accurate depth correction for crack shape impossible.

For deep, through-plate-width cracks, the measured potentials appear to be affected by the location of the probe. Probes close to the specimen edge produce higher potentials and there is also a significant drop in measured potentials in the right half of the plate (probes No. 11-19 compared with No. 1-9). These variations can be clearly seen in Fig. 9d-f.

To avoid the inaccuracies associated with the use of theoretical equations, an individual calibration curve (Fig. 4) for each probe pair determined from beach mark depth measurements (beneath the probes), has been used to convert measured potentials into crack depth. The measured crack depth from a probe pair closest to the first initiating (and initially the deepest) crack, as a function of number of cycles is shown in Figs. 10a-c for stress ranges of

100, 150 and 200 MPa respectively. The curves clearly show the decrease of both initiation and total fatigue lives with increasing thickness. The initiation lives, given in Table 4, were determined from an enlarged a vs N diagram.

The 103 mm plate used for making the thickest joints was delivered, by error, in the as-rolled rather than the normalized state. The resulting lack of toughness was shown by brittle pop-ins which occurred in all 103 mm joints tested. In the T3E specimen tested at $\Delta\sigma$ = 70 MPa, the brittle pop-in shown in Fig. 11 occurred at the maximum crack depth of 11.5 mm. It did not extend to the plate surface; the arrest at both ends is marked by steps. In the depth direction the length of the pop-in varied from 5 to 10 mm. After pop-in, the fatigue crack propagated past the plate half thickness, and terminated in a brittle fracture which severed the plate in two. In joint T1E, tested at a higher stress range (100 MPa), pop-ins extended along the whole crack front (Fig. 12a,b). The brittle crack gradually changed direction of propagation, as shown in the side view of the crack in Fig. 13, until it propagated parallel to the base plate surface and arrested. In joint T2E tested at 150 MPa the fatigue crack turned into a brittle fracture at about the same crack depth and the brittle crack propagated in a similar fashion i.e. turning to become parallel with the base plate surface in mid-thickness. Only one, brief brittle crack arrest occurred after about 25 mm of propagation.

Dimensions of cracks at the first pop-ins in terms of depth a and aspect ratio $\frac{a}{c}$, the maximum, the maximum stresses, and calculated stress intensity factors K_{1c} are given in Table 6. The K_{1c} values were calculated for both 2-D cases (assuming straight-fronted cracks with depth a) and 3-D cases (assuming semi-elliptical crack with max. depth a, and surface length 2c) using calibration data from Ref. [10].

The a vs N curves for these brittle joints, with marked crack extensions from brittle pop-ins, are shown in Fig. 14. It is interesting to note that for the specimen tested at $\Delta\sigma$ = 70 MPa, where the brittle crack extension was embedded inside the plate (see Fig. 11), the increase in potential, immediately following pop-in was minimal. The pop-in was marked on potential

or crack growth curves only by a faster fatigue crack growth rate over the brittle pre-cracked area. In the specimen tested at $\Delta\sigma$ = 100 MPa, where the brittle crack extended along the whole length of the crack front, the pop-in was immediately followed by a substantial jump in potential. However, the full potential increase corresponding to actual crack extension developed only after several hundred fatigue cycles were applied after crack arrest. These observations suggest that tightly closed cracks with clean matching surfaces are permeable to AC current, and that ACPD technique will not detect internal brittle pop-ins.

The brittle fractures initiated from relatively deep fatigue cracks. It means that the major part of the fatigue life was already spent, and that the reduction of total fatigue lives was minor. From extrapolation and comparison with crack-growth curves for other specimens it can be estimated that the total fatigue life reduction from brittle fracture was less than ten per cent.

DISCUSSION AND CONCLUSIONS

As stated in the introduction the objective of this report is to present data on fatigue life and fatigue crack growth measured on welded plate T-joints over a wide range of thicknesses. Final analysis of the effect of thickness on fatigue life will be done after the data given here are combined with the results of a similar set of tests carried out by AMCA/University of Waterloo. The fatigue crack development and fracture mechanics prediction of fatigue life have been already reported in Ref. [7]. Thus only a brief discussion, and summary of the results is in order here.

As can be seen from Table 4, and Figs. 7,10, the total fatigue life is significantly reduced as plate thickness increases. The fatigue life reduction is comparable with that measured in other experimental studies [2-6].

The 0.5 mm cracks initiated early in all tests, at 16 to 35% of endurance (Table 4). In other studies crack detection was reported at 13 to 80% of endurance [2-6].

The compliance measurements presented in Table 4, show that significant change in displacement range occurs only after a deep crack is present in the plate, i.e. when over 70% of the fatigue life has been spent.

The thickness effect is correctly predicted by fracture mechanics if the same initial defect size is assumed for all thicknesses [2,7,10]. With the same weld-toe geometry for all thicknesses (Table 3), stress concentration and distance over which the high stresses spread, increases with thickness as seen in Fig. 5. Assuming that a similar stress distribution applies through the thickness, it can be seen that a 1 mm deep crack will be subject to almost twice as high stress in a 103 mm thick joint than in a 16 mm one. This results in faster growth of small cracks in thicker plates and consequently in shorter life.

The 103 mm thick joints made from as-rolled plate experienced extensive brittle pop-ins during fatigue tests. The first pop-ins were triggered by deep fatigue cracks, and the resulting reduction in endurance is estimated to be marginal. The critical stress intensity factors K_{1c}, reported in Table 6 for unknown reasons appear to increase proportionally to maximum stress or stress range.

ACKNOWLEDGEMENT

The authors wish to acknowledge M.J. Pates of AMCA for development of welding procedure and overseeing the manufacturing of welded test joints.

REFERENCES

1. Offshore Installation: Guidance on Design and Construction, New Fatigue Design Guidance for Steel Welded Joints in Offshore Structures, U.K. Department of Energy, HMSO 1984.

2. Berge, S. "Effect of plate thickness in fatigue design of welded structures"; Offshore Technology Conference; Paper 4829; Houston; May 1984.

3. Morgan H.G. "The effect of section thickness on the fatigue performance of simple welded joints"; Report ND-R941(S); UKAEA; HMSO London; Oct. 1983.

4. Webster, S.E., Austen, I.M, and Rudd, W.J. "Fatigue corrosion fatigue and stress corrosion of steels for offshore structures"; British Steel Corp.; Report Ref: FR 103-6/832, for ECSC Sponsored Res. Project; April 1984.

5. de Back, J. and Vaessen, G.H.G. "Effect of plate thickness, temperature and weld toe profile on the fatigue and corrosion fatigue behaviour of welded offshore structures"; Report for ECSC Convention 7210-KG/601 by Foundation for Materials Research in the Sea; Delft, Netherlands; May 1984.

6. Booth C.S. "The influence of thickness on the fatigue strength of welded plate specimens" The Welding Institute Report No. 3733/10/84 for UKAEA; Sept. 1984.

7. Vosikovsky, O., Bell, R., Burns, D.J. and Mohaupt, U.H. "Fracture mechanics assessment of fatigue life of welded plate T-joints, including thickness effect"; Proceedings of the 4th International Conference on Behaviour of Offshore Structures; Delft, Netherlands; July 1-5, 1985.

8. Charlesworth, F.D.W. and Dover, W.D. "Some aspects of detection and sizing using AC field measurements"; Advances in Crack Length Measurement; Editor G.J. Beevers, 253-276; EMAS; 1982.

9 Vosikovsky, O. and Rivard, A. "Fatigue crack propagation in welded plate T-joints, interim report"; PMRL Report ERP/PMRL 84-30(TR); May 1984.

10. Bell, R. "Determination of stress intensity factors for weld toe defects, Phase II; CANMET Contract Report by Centre for Advanced Engineering Design; Carleton University, Ottawa; DSS File No. 22ST. 23440-2-9083/11; Oct. 1985.

Table 1 - Chemical composition and mechanical properties

Chemical composition	Plate thickness (mm)				
	16	26	52	78	103
C	0.07		0.12		0.13
Mn	1.40		1.39		1.43
Si	0.29		0.28		0.23
S	0.005		0.011		0.003
P	0.004		0.017		0.013
Al	0.045		0.027		0.015
Ni	0.25		0.15		0.24
Cr	0.25		0.17		-
Mo	-		$\leq$0.01		-
Cu	-		0.15		-
Ti	0.012		-		0.006
V	0.075		0.053		0.06
Nb	0.022		0.041		0.02
N	0.01		-		0.01
Mechanical Properties:					
Yield Strength (MPa)	421	405	390	370	350
UTS (MPA)	509	513	517	505	502
Elongation (%)	53	29	32	31	38

Table 2 - Welding variables (refer to Fig. 2)

Pass No.	Side No.	Welding process	Welding position	Electrode Size (mm)	Type	Classification	Polarity	Amps	Volts	T.S (mm)
1-2	1	SMAW	3G	3.2	CLA	E7018	DC+	115/125	20/23	110/120
3-4	2	SMAW	3G	3.2	CLA	E7018	DC+	115/125	20/23	110/120
5-6	1	SMAW	3G	4.0	CLA	E7018	DC+	160/175	20/23	110/120
7-8	2	SMAW	3G	4.0	CLA	E7018	DC+	160/175	20/23	110/120
9-10	1	SMAW	3G	4.0	CLA	E7018	DC+	160/175	20/23	110/120
11	1	SMAW	3G	3.2	CLA	E7018	DC+	115/125	20/23	110/120
12/13	2	SMAW	3G	4.0	CLA	E7018	DC+	160/175	20/23	110/120
14/18	1	SMAW	3G	3.2	CLA	E7018	DC+	115/125	20/23	110/120
19	2	SMAW	3G	4.0	CLA	E7018	DC+	160/175	20/23	110/120
20/26	2	SMAW	3G	3.2	CLA	E7018	DC+	115/125	20/23	110/120

Note: Pass sequence varied to balance heat affecting vertical member of tee. Also, a dime test requirement was imposed on weld toe.

Plate Thickness (mm)	Preheat (°C)	Interpass (°C)	Average No. of passes
16	RT	230	11
26	15	230	26
52	70	230	55
78	120	230	120
103	120	230	200

Table 3 - Weld toe geometry of tested specimens

Spec. No.	t (mm)	ℓ (mm)	θ_{min} (deg)	θ_{max} (deg)	$\bar{\theta}$ (deg)	S_θ (deg)	r_{min} (mm)	r_{max} (mm)	$\bar{r}$ (mm)	S_r (mm)
T1A	16	11	34	47	40	4	0.4	2.0	1.2	0.5
T2A	16	10	30	44	38	5	0.4	2.4	1.5	0.7
T4A	16	11	31	51	40	6	0.4	2.0	1.2	0.6
T7B	26	17	35	50	42	6	0.2	2.2	1.3	0.7
T8B	26	17	32	46	38	5	0.3	3.2	1.3	0.8
T9B	26	15	33	38	36	2	0.7	3.0	1.6	0.7
T1C	52	32	33	57	39	8	0.5	3.3	1.3	1.1
T2C	52	32	33	55	41	7	0.5	1.8	1.1	0.5
T3C	52	29	33	45	39	4	0.2	3.0	1.1	1.0
T1D	78	39	39	52	46	5	0.2	2.0	0.9	0.6
T2D	78	37	40	62	46	8	0.3	2.5	1.8	0.5
T3D	78	39	36	69	46	11	0.8	3.0	1.9	0.8
T1E	103	51	31	53	40	8	0.3	3.0	1.5	1.3
T2E	103	55	30	72	45	15	1.0	3.0	1.7	0.7
T3E	103	58	36	52	43	5	0.5	2.4	1.5	0.6

Table 4 - Endurance and fatigue crack initiation lives of the specimens tested

Spec/ Thick-ness (mm)	Stress range - (MPa)			Endurance $a_f = t/2$ (kc)	Initiation $a_i = 0.5$ mm	
		Measured †				
	Calcu-lated	Test weld toe	Ground weld toe		(kc)	% end.
T1A/16	100	100.4	98.3		>3500	
T4A/16	110	107.6	106.5		>3050	
T2A/16	150	151.6	150.6	1270	320	26
T1A/16	200	198.7	198.7	460	147	32
T8B/26	100	95.8	95.5	3910	1130	28.9
T9B/26	150	143.6	143.4	1125	390	34.7
T7B/26	200	195.7	196.2	336	88	26.2
T1C/52	100	99.3	95.8	1210	380	31.4
T2C/52	150	145.5	141.4	370	90	24.3
T3C/52	200	197.7	190.5	137	37	27.0
T1D/78	100	98.9	99.3	1257	260	20.4
T3D/78	150	143.9	138.8	282	70	24.8
T2D/78	200	199.2	198.4	97	25	25.8
T3E/103	70	70.	66.6	2380*	390	16.4
T1E/103	100	100.0	100.0	660*	160	24.2
T2E/103	150	150.1	150.1	167*	45	26.9

*Brittle fracture pop-ins

†by extrapolation using strain gauges

Table 5 - Number of cycles and maximum crack depth at the first detectable increase in actuator displacement range

Spec/t (mm)	Stress range (MPa)	No. of cycles (k cycles)	Endurance (%)	Max. crack depth (mm)
T2A/16	150	960	75.6	4.9
T1A/16	200	350	76.1	3.2
T8B/26	100	3250	83.1	8.8
T9B/26	150	860	76.4	4.9
T7B/26	200	270	80.4	4.6
T1C/52	100	1000	82.6	8.2
T2C/52	150	310	83.9	13.6
T3C/52	200	100	73.0	7.0
T1D/78	100	960	76.4	10.3
T3D/78	150	210	74.5	10.0
T2D/78	200	60	61.9	7.4
T1E/103	100	580	87.9*	15.5
T2E/103	150	155	92.8*	14.8

*Brittle fracture pop-ins

Table 6 - Crack dimensions and stress intensity factors, calculated for straight-fronted (2-D) and semi-elliptical (3-D) cracks, for the first brittle pop-in in 103 mm thick joints

Spec.	Maximum stress σ_{max}-(MPa)	Crack depth a-(mm)	Aspect ratio $\frac{a}{c}$	K_{1c} 2-D (MPa$\sqrt{m}$)	K_{1c} 3-D (MPa$\sqrt{m}$)
T3E	73.7	11.5	.26	18.5	13.7
T1E	105.3	21.0	.24	33.5	20.8
T2E	157.9	18.0	.20	47.7	32.6

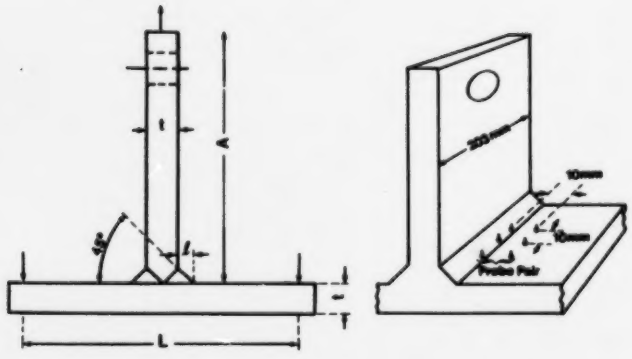

JOINT	t (mm)	l (mm)	L (mm)	A (mm)
A	16	8-12	300	406
B	26	14-18	442	406
C	52	26-30	442	406
D	78	38-42	584	457
E	103	52-56	726	457

Fig. 1 - Geometry and dimensions of tested T-joints, and location of ACPD probes.

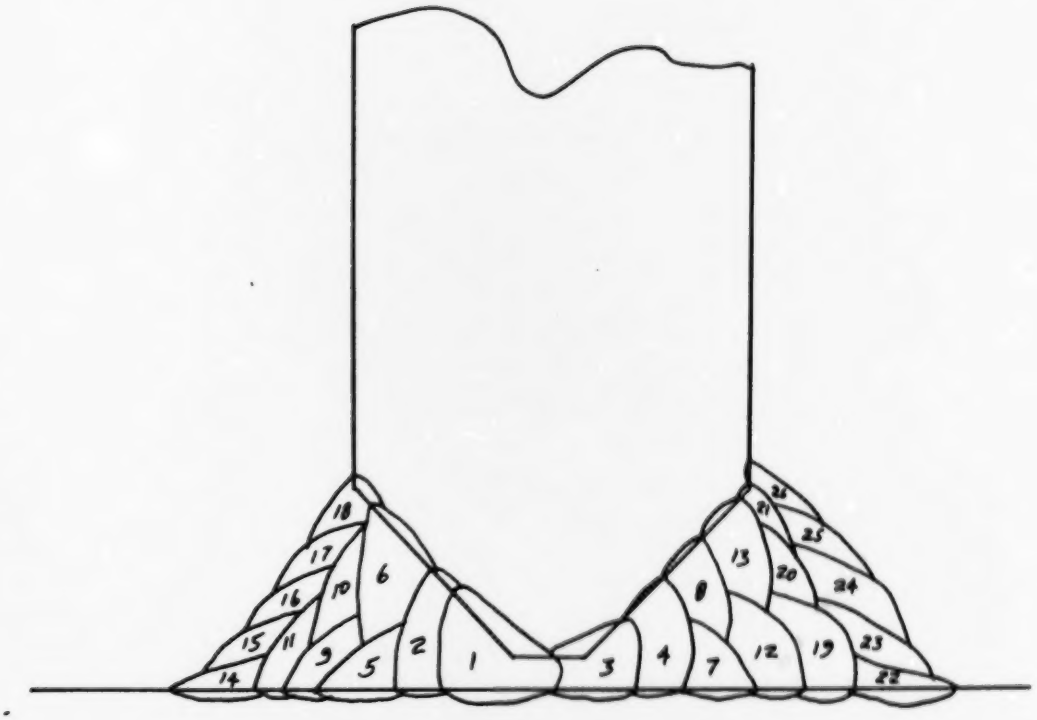

Fig. 2 - Preparation of weld, and typical weld pass sequence, for 26 mm thick T-joint.

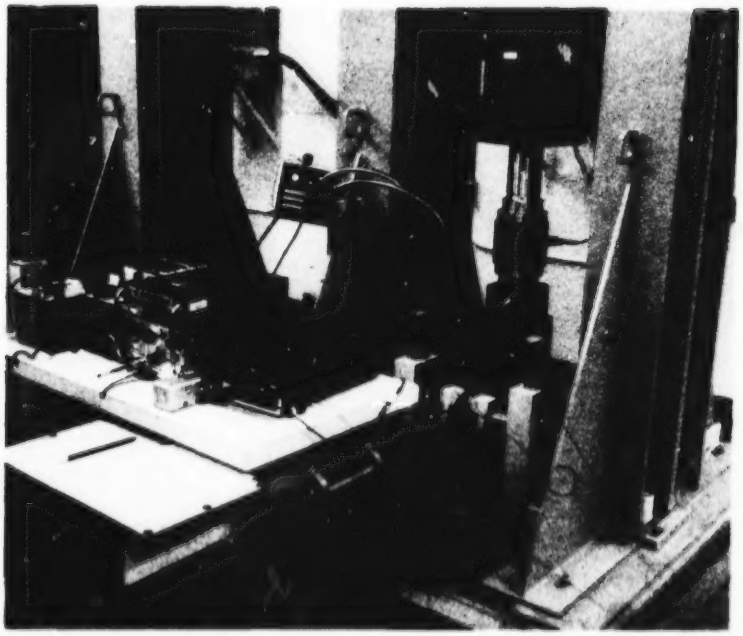

Fig. 3 - T-joint in a test frame with ACPD measurement instruments.

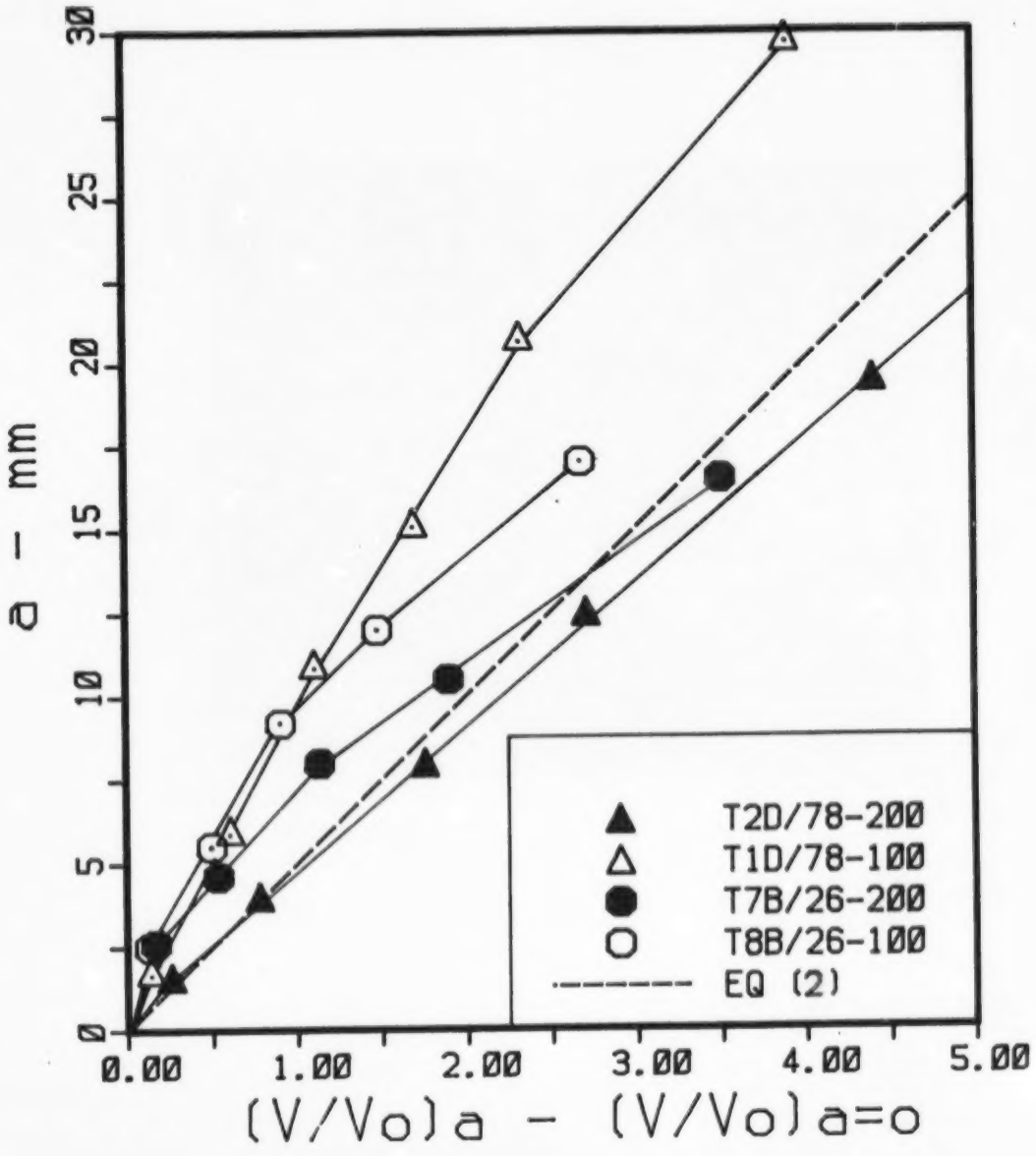

Fig. 4 - Calibration curves for probe nearest to the deepest point of crack in specimens 26 and 78 mm thick, tested at 100 and 200 MPa stress ranges. The dashed line is the theoretical calibration curve for straight-fronted crack corresponding to Eq (2) with A = 5.

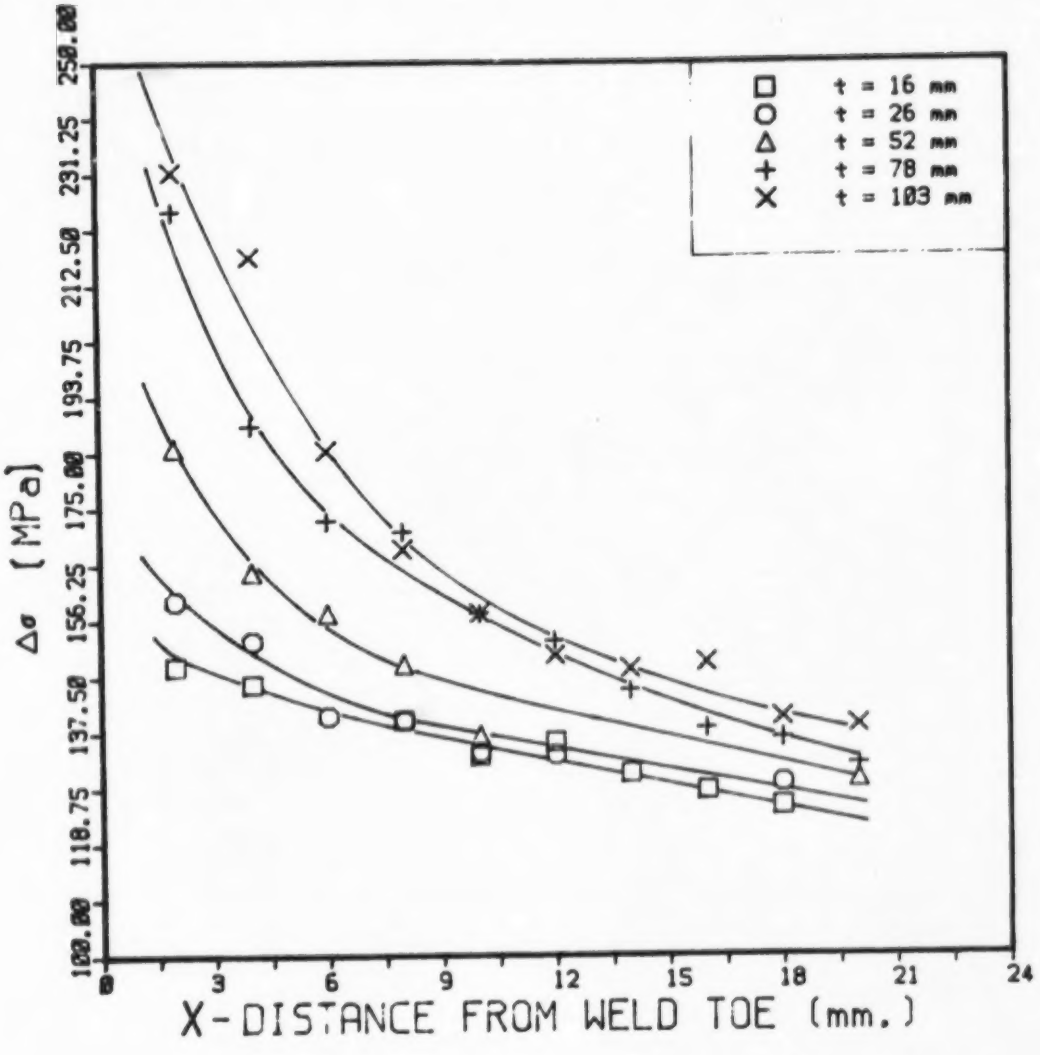

Fig. 5 - Distributions of stress near weld toe for five joint thicknesses at nominal $\Delta\sigma$ = 150 MPa.

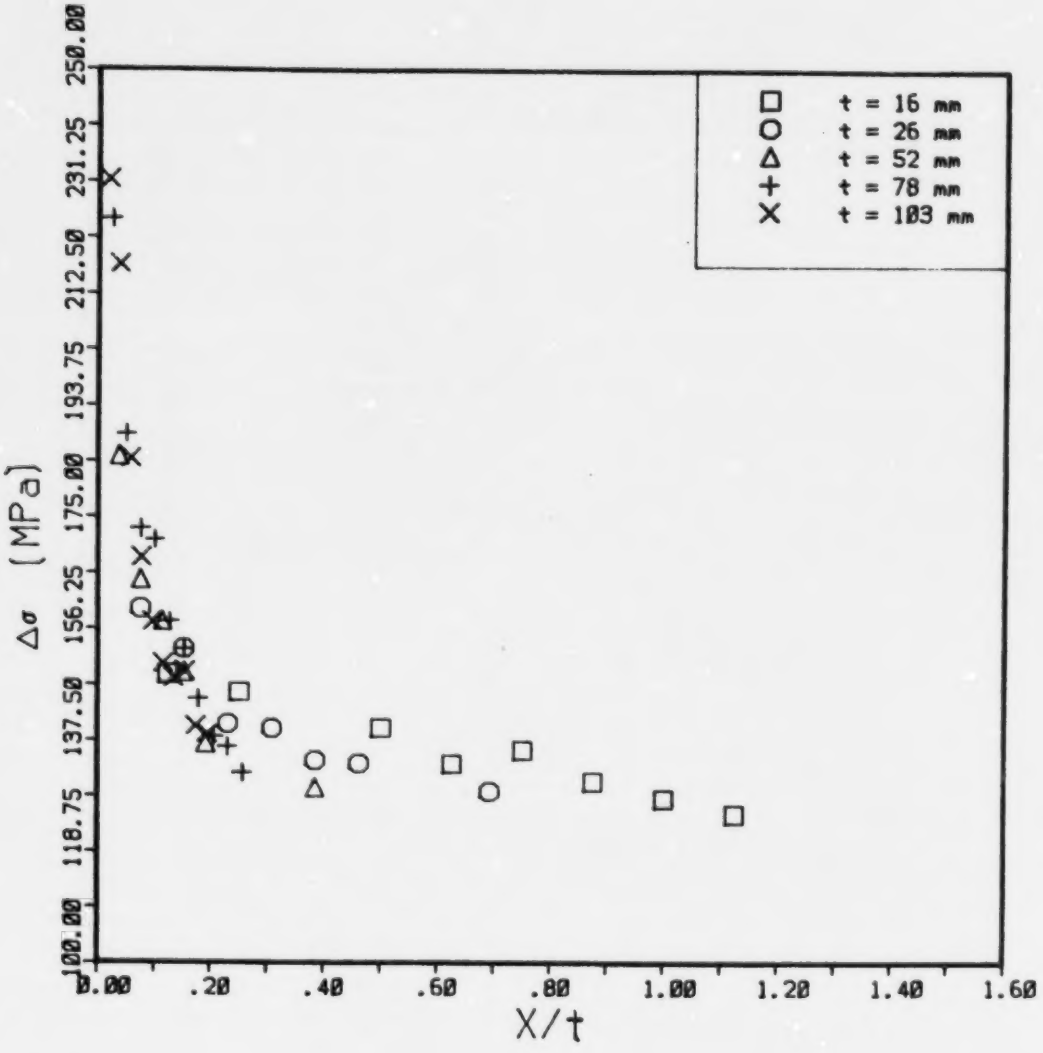

Fig. 6 - Distribution of stress near weld toe as a function of distance x divided by plate thickness at nominal $\Delta\sigma$ = 150 MPa.

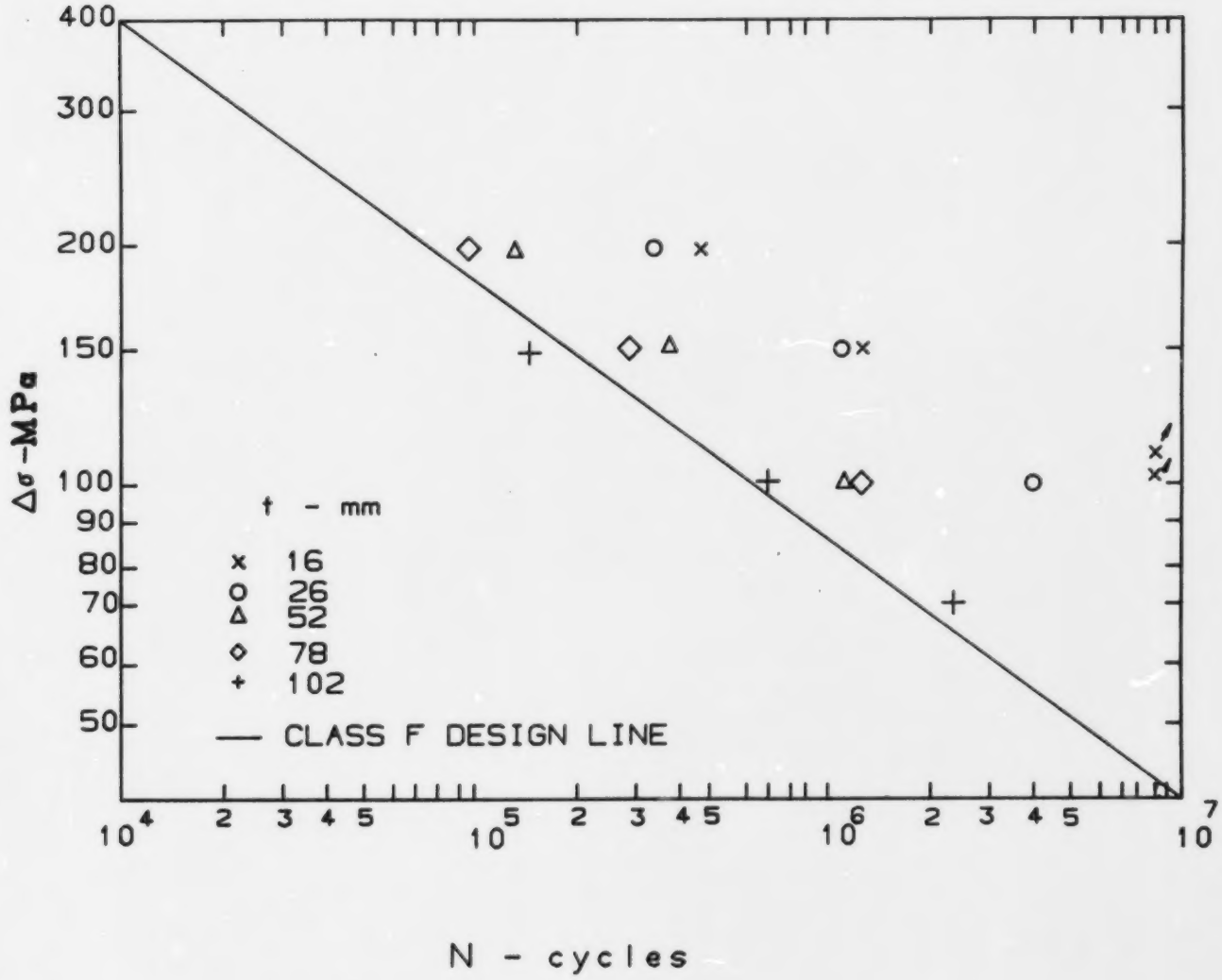

Fig. 7 - Endurances of specimens tested showing effect of thickness t.

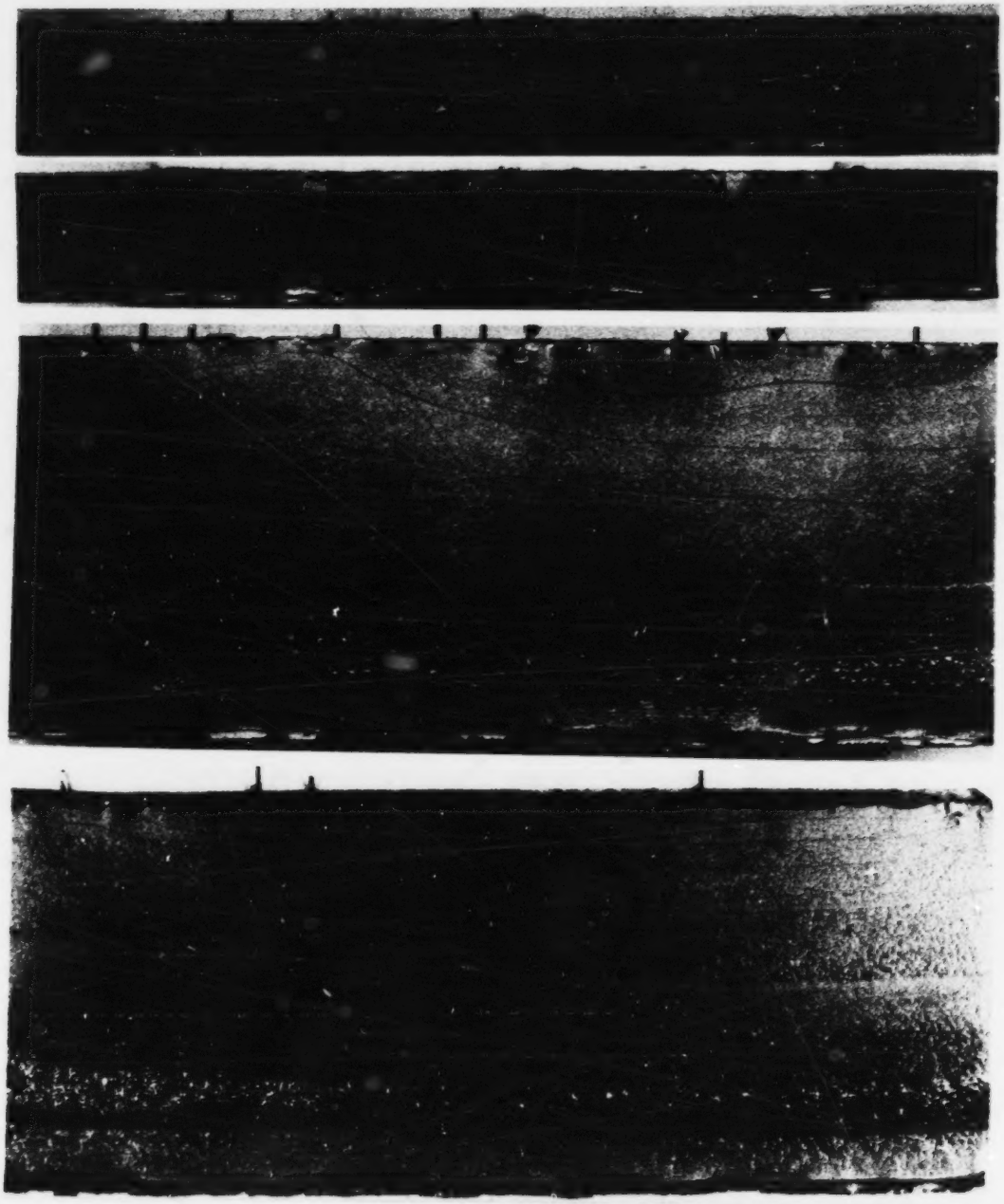

Fig. 8 - Examples of variation in number and shape of cracks with stress range and thickness:

a) $\Delta\sigma$ = 100 MPa, t = 26 mm

b) $\Delta\sigma$ = 200 MPa, t = 26 mm

c) $\Delta\sigma$ = 100 MPa, t = 78 mm

d) $\Delta\sigma$ = 200 MPa, t = 78 mm

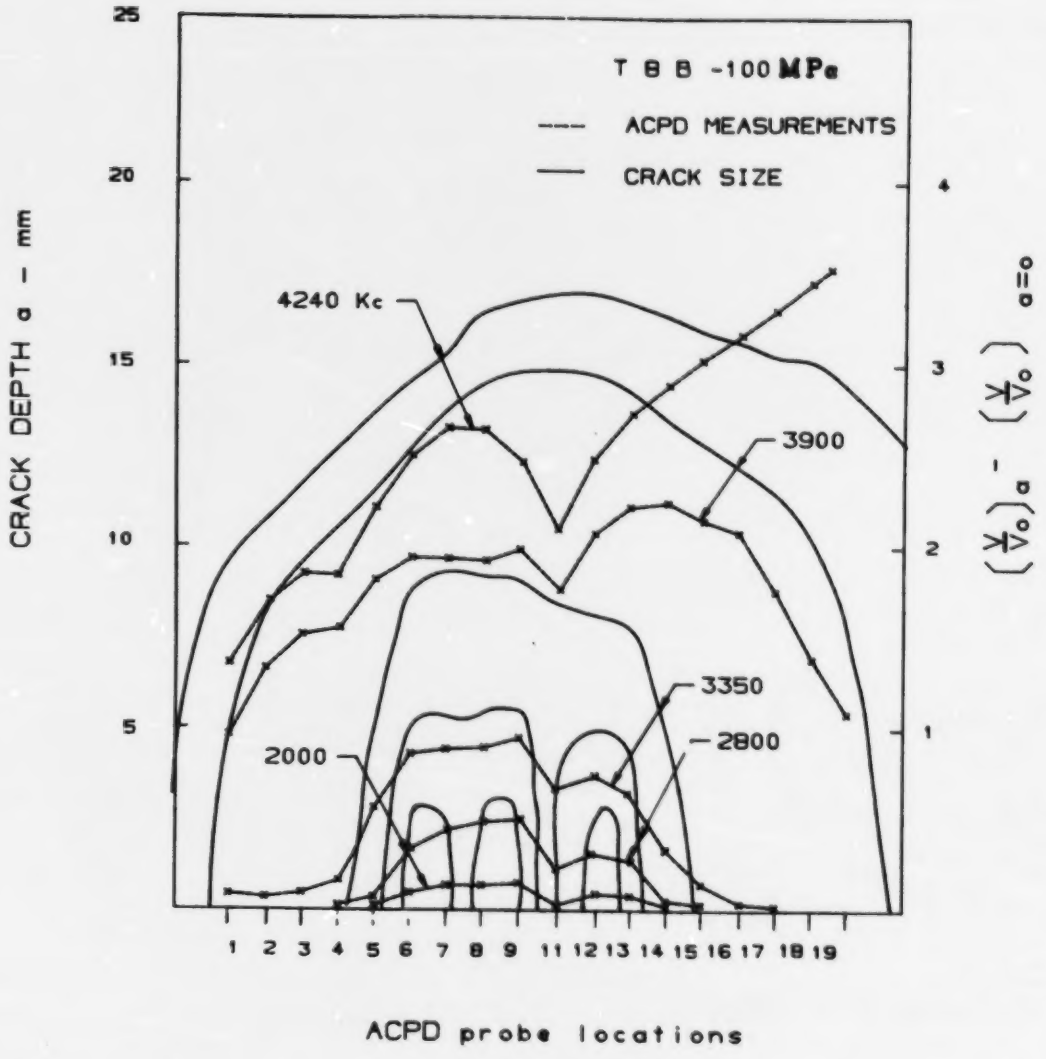

a) t = 26 mm, $\Delta\sigma$ = 100 MPa

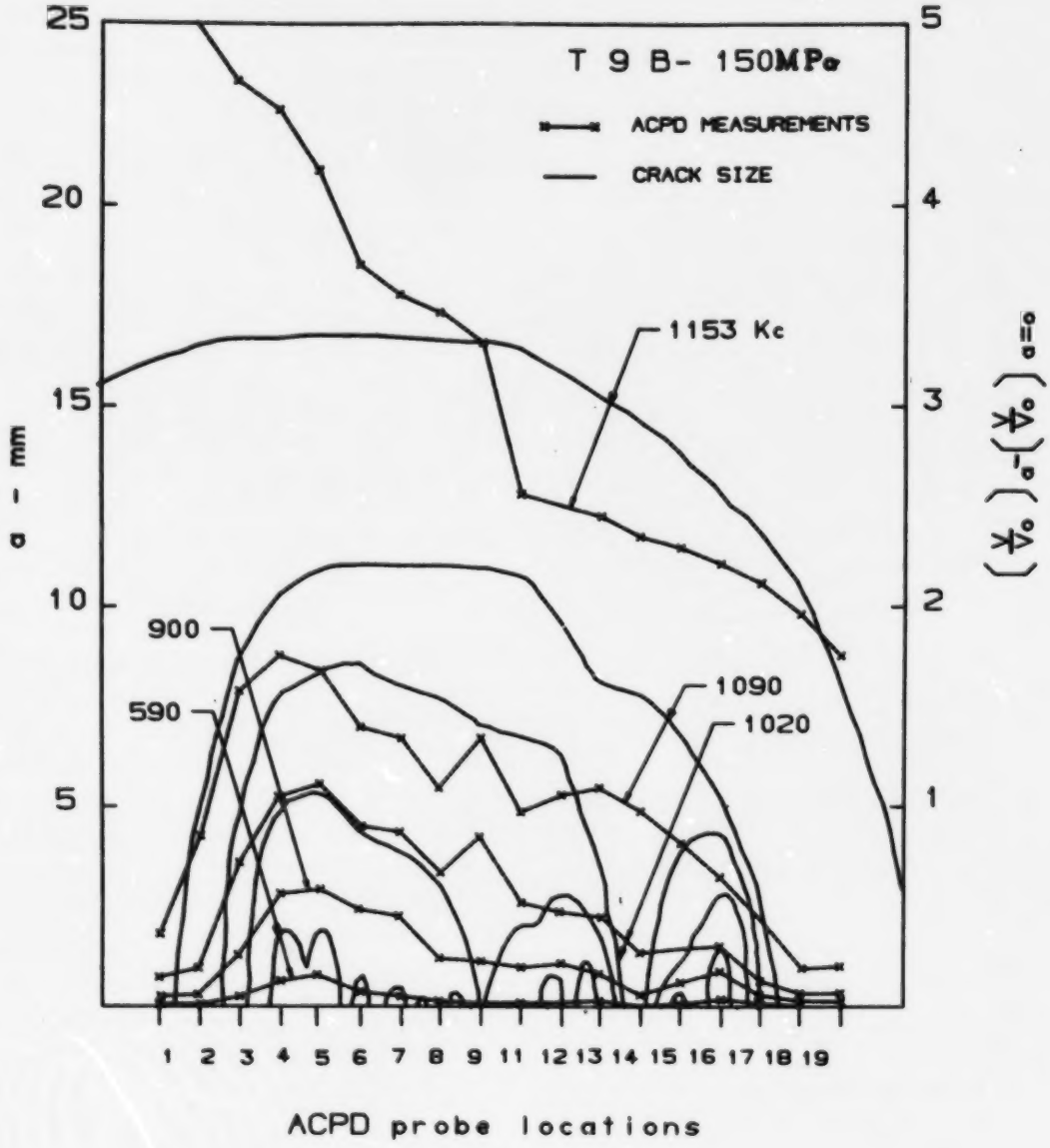

b) t = 26 mm, $\Delta\sigma$ = 150 MPa

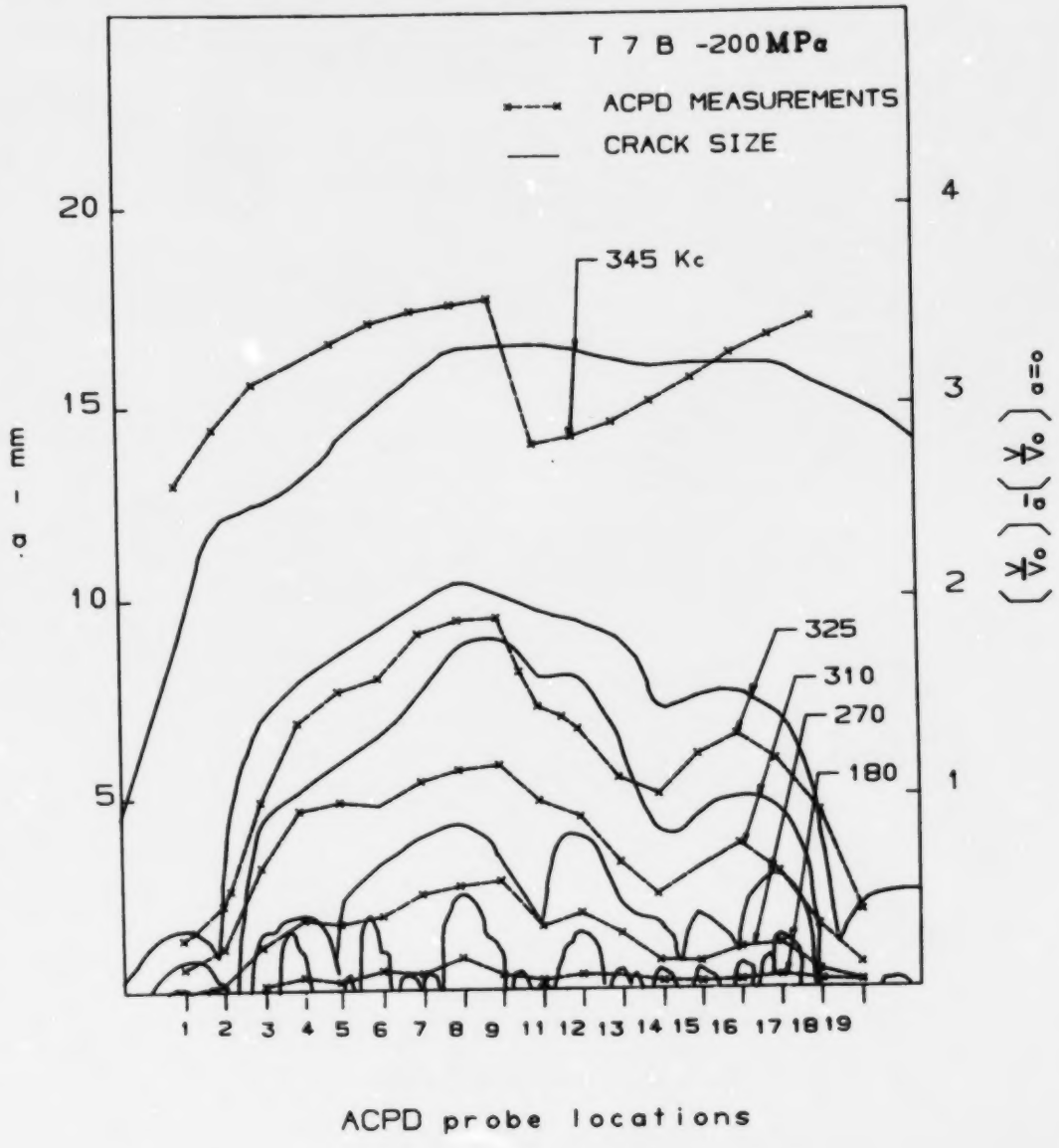

c) t = 26 mm, $\Delta\sigma$ = 200 MPa

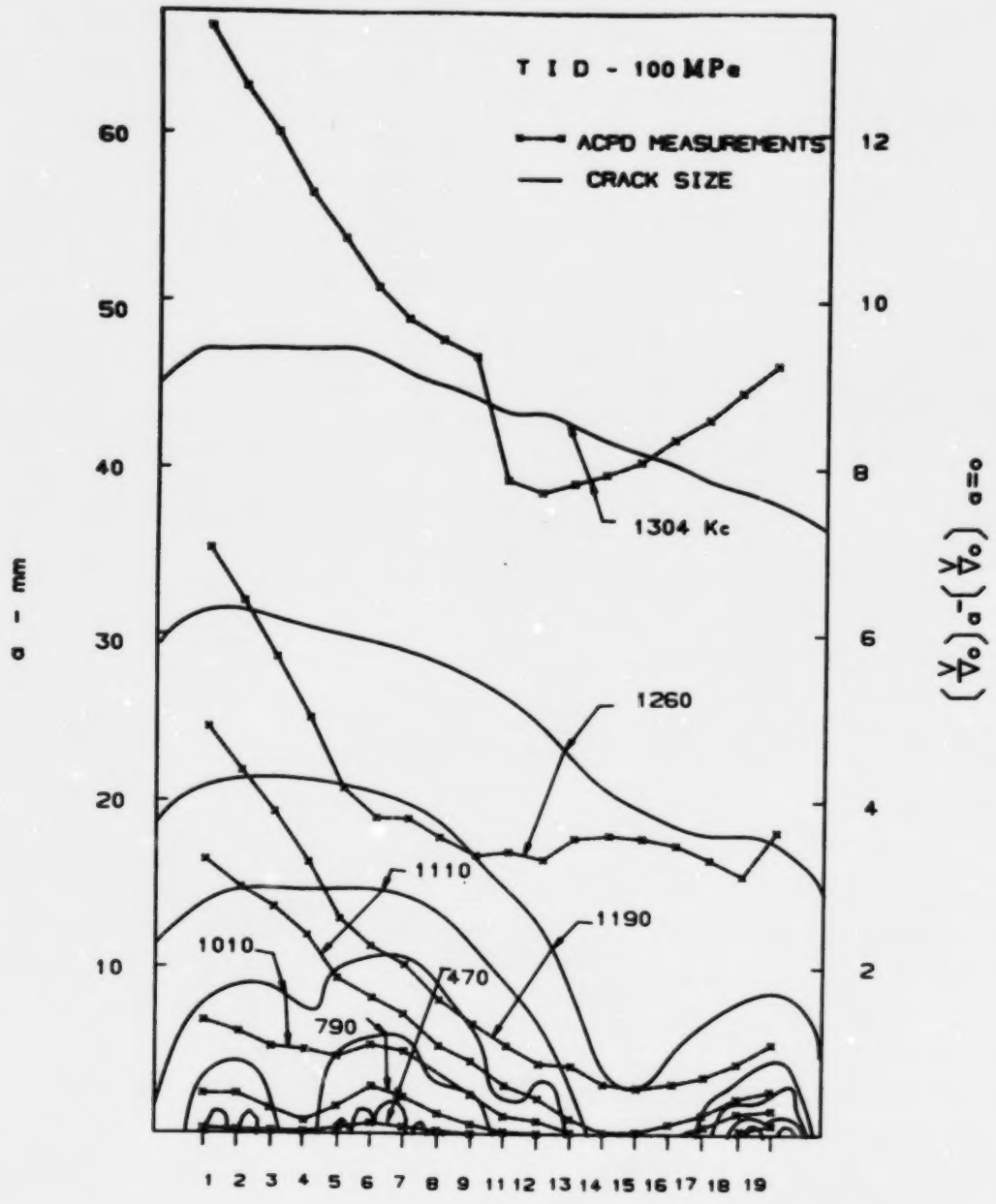

d) t = 78 mm, $\Delta\sigma$ = 200 MPa

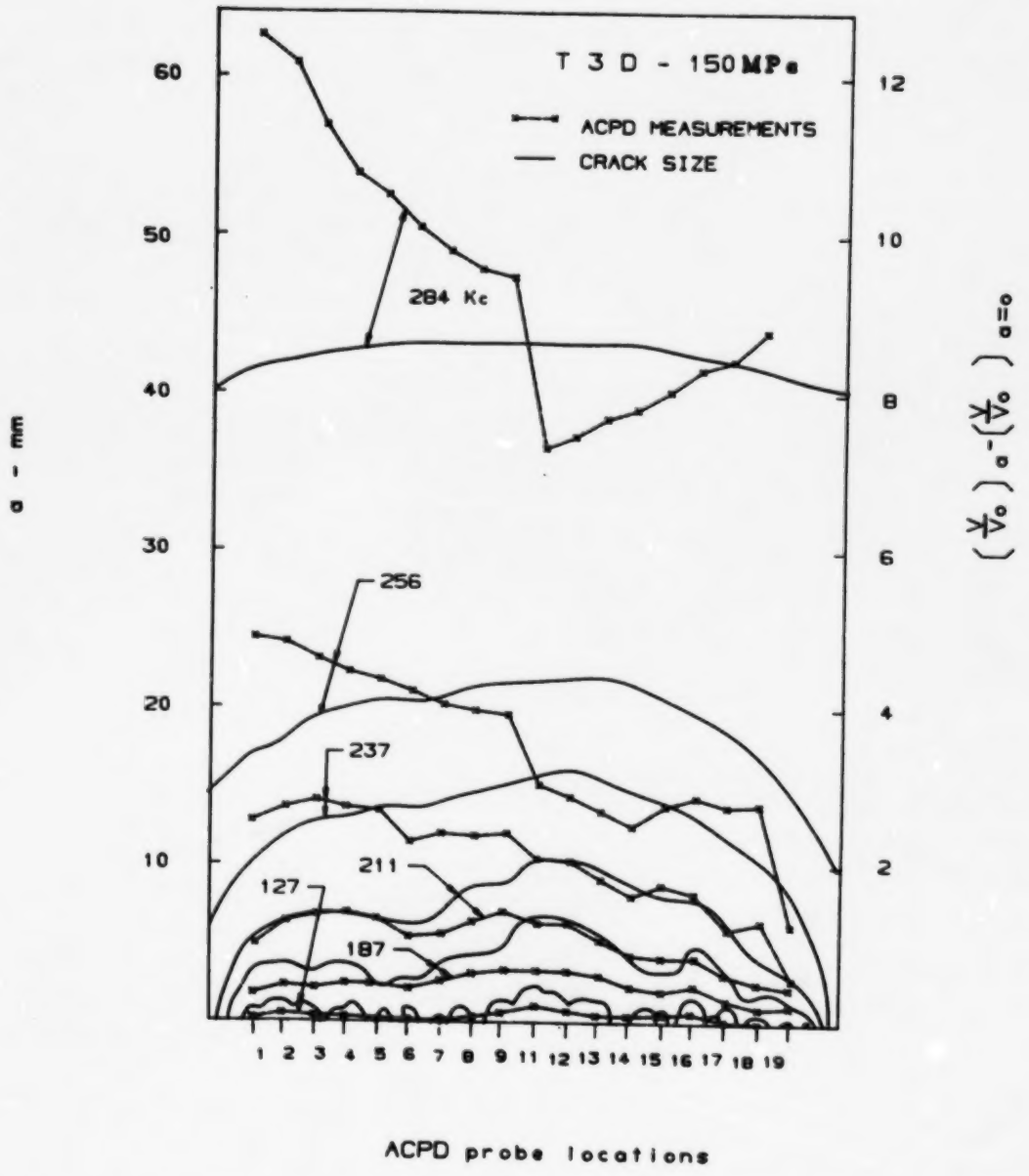

e) t = 78 mm, $\Delta\sigma$ = 200 MPa

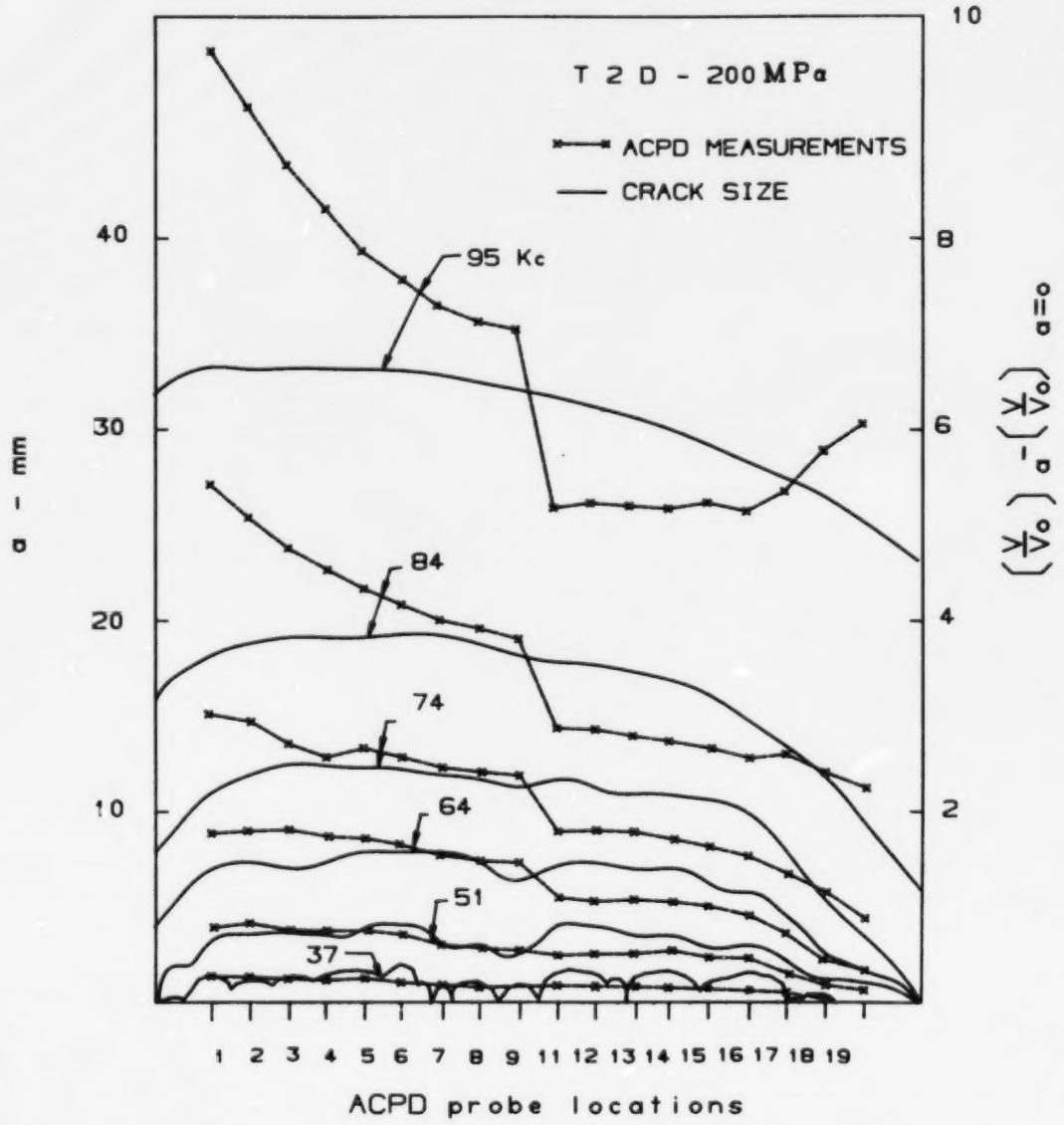

f) t = 78 mm, $\Delta\sigma$ = 200 MPa

Fig. 9 - Comparison of ACPD variations along beach marks with actual crack sizes for the following specimen thicknesses and stress range:

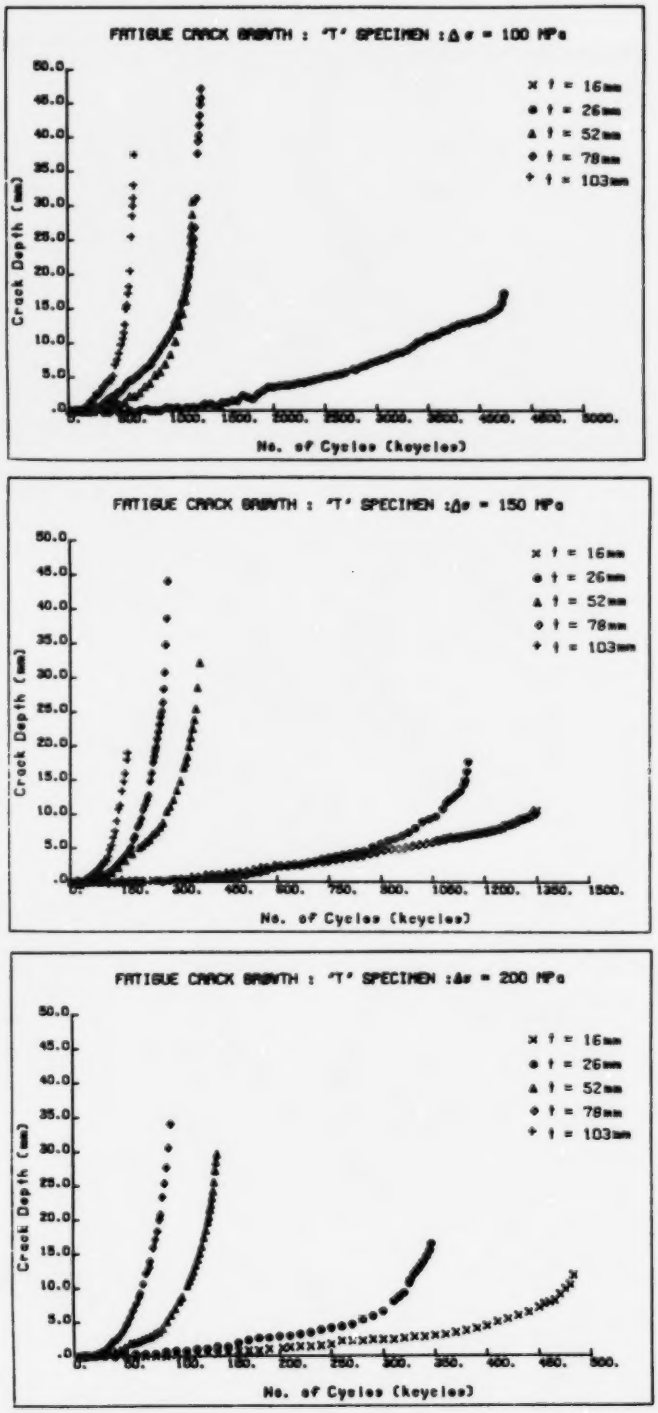
FATIGUE CRACK GROWTH : 'T' SPECIMEN :Δσ = 100 MPa
Crack Depth (mm)
No. of Cycles (kcycles)
× t = 16mm
● t = 26mm
▲ t = 52mm
◆ t = 78mm
+ t = 103mm
FATIGUE CRACK GROWTH : 'T' SPECIMEN :Δσ = 150 MPa
Crack Depth (mm)
No. of Cycles (kcycles)
× t = 16mm
● t = 26mm
▲ t = 52mm
◆ t = 78mm
+ t = 103mm
FATIGUE CRACK GROWTH : 'T' SPECIMEN :Δσ = 200 MPa
Crack Depth (mm)
No. of Cycles (kcycles)
× t = 16mm
● t = 26mm
▲ t = 52mm
◆ t = 78mm
+ t = 103mm

Fig. 10 - The effect of thickness on fatigue crack growth:

a) $\Delta\sigma$ = 100 MPa

b) $\Delta\sigma$ = 150 MPa

c) $\Delta\sigma$ = 200 MPa

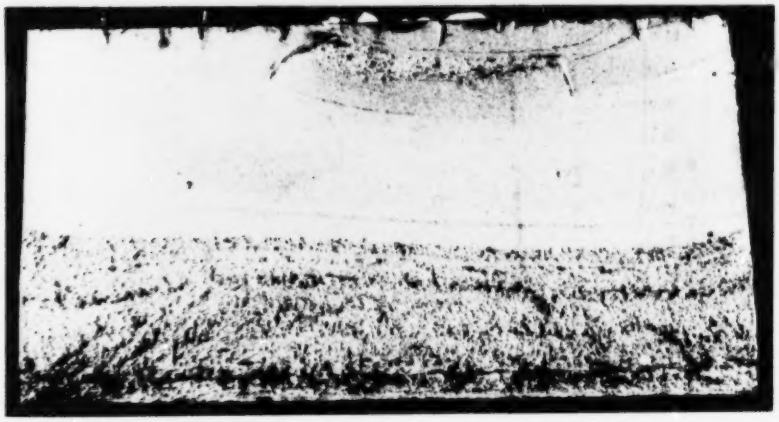

Fig. 11 - Brittle fracture pop-in in the T3E specimen tested at $\Delta\sigma$ = 70 MPa.

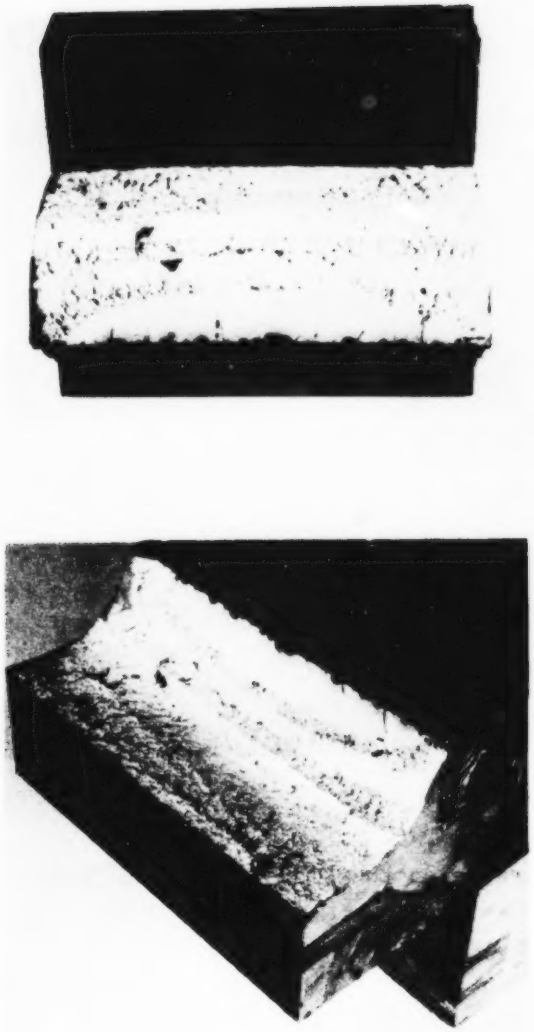

Fig. 12 - Brittle fracture pop-ins in the TIE joint tested at $\Delta\sigma$ = 100 MPa.

a) Fracture on the part containing weld.

b) Fracture on the opposite part of base plate.

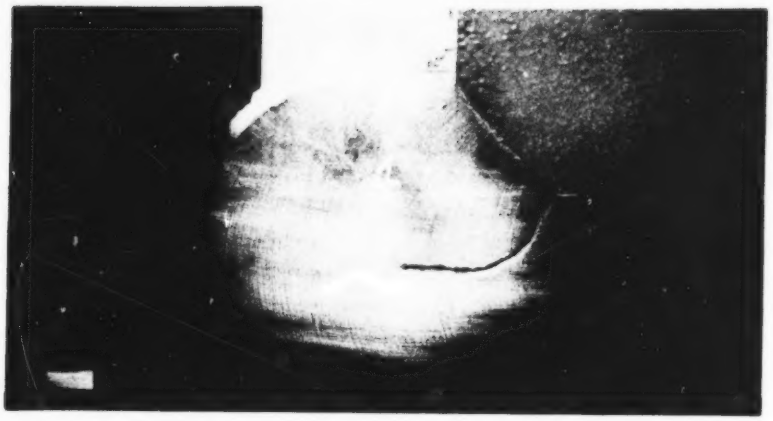

Fig. 13 - Crack appearance on the side of the TIE joint tested at $\Delta\sigma$ = 100 Mpa.

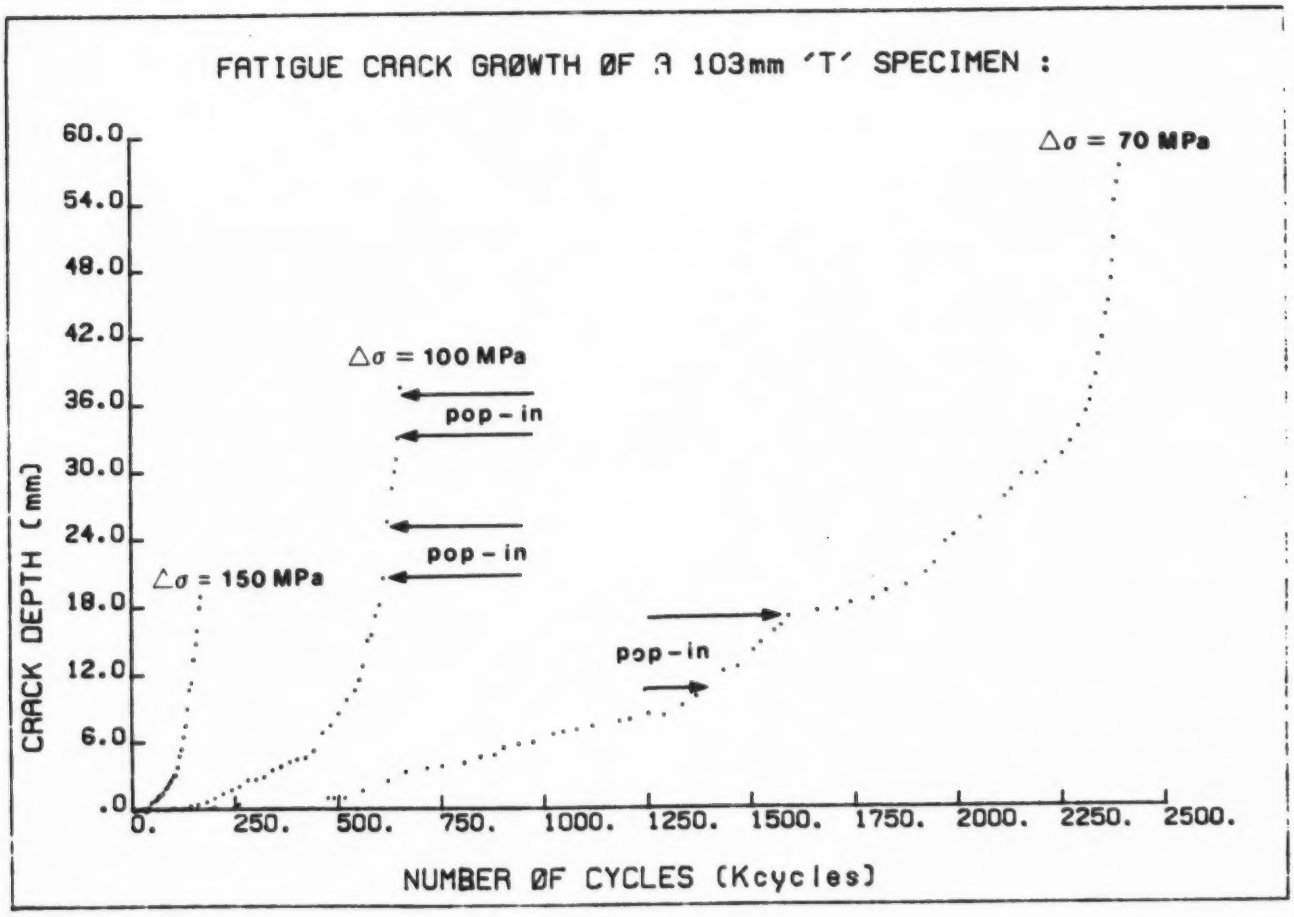

Fig. 14 - The effect of stress range on fatigue crack growth in 103 mm thick T-joints exhibiting brittle fracture pop-ins during crack growth.